Research Article

applied optics

Estimation precision for a normalized response matrix in linear polarization calibration

Xinkai Li,[1] Pengfei Miao,[2] Lingping He,[1] Heng Shen,[1] Xiaodong Wang,[1] Bowen Gong,[1,3] Xingjun Gao,[4] and Bo Chen[1,*]

[1]Changchun Institute of Optics, Fine Mechanics and Physics, Chinese Academy of Sciences, Changchun 130033, China
[2]Shanghai Institute of Satellite Engineering, Shanghai 200000, China
[3]University of Chinese Academy of Sciences, Beijing 100049, China
[4]Research Institute of Intelligent Sensing, Zhejiang Lab, Hangzhou 310000, China
*Corresponding author: chen_bo_2019@163.com

Received 31 May 2022; revised 16 July 2022; accepted 16 July 2022; posted 18 July 2022; published 2 August 2022

The purpose of polarization calibration is to obtain the response matrix of an instrument such that the subsequent observation data can be corrected. The calibration precision, however, is partially restricted by the noise of the detector. We investigate the precision of the normalized response matrix in the presence of signal-independent additive noise or signal-dependent Poisson shot noise. The influences of the source intensity, type of noise, and calibration configuration on the precision are analyzed. We compare the theoretical model and the experimental measurements of the polarization calibration to show that the relative difference between the two is less than 16%. From this result, we can use the model to determine the minimum source intensity and choose the optimal configurations that provide the required precision.

https://doi.org/10.1364/AO.465538

1. INTRODUCTION

Polarization imaging technology is widely used in various fields, including astronomy [1–3], biology [4], medicine [5], agriculture [6], and the military field [7]. Polarization calibration configurations are formed with well-chosen angles to correct the instrument depending on the Stokes–Mueller method [3]. In most cases, the first three elements of the Stokes vector are considered to be due to the zero value of circular polarized element [3,8]. The noise of the detector determines the precision that the polarization imager achieves; therefore, we can choose optimal calibration configurations according to the detector noise.

In recent years, Foreman found that the distribution of the optimal analysis states over the Poincaré sphere is described by a regular polygon [9]. The equivalence of an optimization has been established based on the equally weighted variance and the condition number κ of the associated response matrix. The estimation variance increases with the number of measurements N when the noise is additive; it is independent of N in the presence of Poisson shot noise and decreases with N when the angles of the analyzers fluctuate [10]. They also proposed a set of polarization states whose estimation precision depends on the observed Mueller matrix only through its intensity reflectivity, not through its other polarimetric properties in the full polarization frame [11]. Furthermore, Goudail demonstrates that the architectures that minimize and equalize the estimation variances for both types of noise are based on spherical designs of order 2 or 3 over the Poincaré sphere [12]. The optimal reference polarization states have been derived, and the analytical results were verified via simulations and experiments [13]. It is noted that the influence of incident light is analyzed, and the effective calibration method can be used to ensure the precision in practice according to different incident polarization states [14].

These references assume that the measured intensities are influenced by Gaussian and Poisson noise, under the condition of the unnormalized response matrix. In practice, the response matrix is usually normalized by the instrument throughput, and the variance of the normalized matrix represents the precision that the polarization calibration can reach [3]. Research on the variance of the normalized response matrix is necessary, and it is helpful to design the polarization calibration scheme in advance according to the detector noise.

In linear polarization calibration, we obtain the estimation variance for the normalized response matrix in the presence of Gaussian and Poisson noise. We shall see that the calibration precision depends on three types of perturbation, namely, the source intensity, configuration, and noise. We compare the theoretical model and the experimental measurements of the polarization calibration to show that the relative difference between the two is less than 16%. From this result, we can use the model to determine the minimum source intensity and choose the optimal configurations that provide the required precision. We verify this conclusion with experiments.

This paper is organized as follows: in Section 2, we describe the model for linear Stokes calibration. Then we obtain the estimation variance of the normalized response matrix in the presence Gaussian and Poisson noise and propose the theoretical prediction model (Section 3). In Section 4 we present the experimental setups, results, discussions, and systematic errors. Finally, we conclude this paper in Section 5.

2. CALIBRATION MODEL FOR LINEAR POLARIZATION POLARIMETER

We consider the linear polarization calibration that performs more than nine intensity measurements. The response matrix of the polarization calibration of the instrument is defined as

$$M = \begin{pmatrix} M_{11} & M_{12} & M_{13} \\ M_{21} & M_{22} & M_{23} \\ M_{31} & M_{32} & M_{33} \end{pmatrix}. \tag{1}$$

The measuring system consists of a light source of the intensity I_0, a polarization state generator (PSG) that illuminates the optical system with special orientation, and a polarization state analyzer (PSA) that is used to analyze the polarization states of light generated by the instrument. A detector is then used to collect the light exiting from the PSA in a particular direction. The intensities acquired from an unpolarized light source I_0 are given by

$$I = I_0 A M G^T, \tag{2}$$

where I is the intensity measured by a detector, which depends on the measurements obtained from the combination of a PSA and PSG, the matrix G (A) which is formed by a PSG (PSA) has the dimensions $N_G \times 3$ ($N_A \times 3$), and the superscript of T, which denotes the transpose of the matrix. To obtain the relationship between I and M, Eq. (2) can be rewritten as follows [11,12]:

$$\mathbf{V}_I = [A \otimes G]\mathbf{V}_M, \tag{3}$$

where $\otimes$ denotes the Kronecker product [15], $\mathbf{V}_M = [(V_M)_1\ (V_M)_2 \cdots (V_M)_9]$ is a nine-dimensional vector, and $\mathbf{V}_I = [(V_I)_1\ (V_I)_2 \cdots (V_I)_{N_G N_A}]$ is a $N_G \times N_A$-dimensional vector. $\mathbf{V}_M$ and $\mathbf{V}_I$ are nine-dimensional vectors obtained by reading matrices $I_0 M$ and I, respectively, in lexicographic order.

In this paper, we investigate the calibration precision in which the response matrix is normalized by the instrument throughput M_{11} (that is, M/M_{11}) in the presence of Gaussian and Poisson noise.

3. PRECISION OF RESPONSE MATRIX IN THE PRESENCE OF GAUSSIAN AND POISSON NOISE

Equation (3) can be rewritten as follows:

$$\mathbf{V}_M = P\mathbf{V}_I, \tag{4}$$

with

$$P = [A \otimes G]^\dagger, \tag{5}$$

where P is the pseudo-inverse matrix. Based on the properties of the Kronecker product [15], the matrix P is rewritten as

$$P = [F_A \otimes F_G][A \otimes G]^T, \tag{6}$$

where $F_U = (U^T U)^{-1}$, and $U = G$ or A. The covariance matrix can then be determined by [16,17]

$$\mathbf{\Gamma}_{\mathbf{V}_M} = P\mathbf{\Gamma}_{\mathbf{V}_I} P^T, \tag{7}$$

where $\mathbf{\Gamma}_{\mathbf{V}_M}$ is the covariance matrix of $\mathbf{V}_M$. A standard scalar performance criterion is the sum of the estimation variance of the response matrix, which is the trace of $\mathbf{\Gamma}_{\mathbf{V}_M}$:

$$C = \mathrm{Tr}[\mathbf{\Gamma}_{\mathbf{V}_M}], \tag{8}$$

where $\mathbf{\Gamma}_{\mathbf{V}_I}$ is the covariance of $\mathbf{V}_I$. I is replaced by R due to the normalization as

$$R = \frac{I}{z}, \tag{9}$$

where z is the value M_{11} for every pixel, and R is a $N_G \times N_A$-dimensional matrix. We obtain the variance of the normalized response matrix from the Taylor series expansion with a first-order approximation:

$$D[R(m,n)] \approx \frac{D[I(m,n)] + R^2(m,n)D(z) - 2RCov[z, I(m,n)]}{z^2}, \tag{10}$$

where $D[I(m,n)]$ is the variance of the measurement intensity, $Cov[z, I(m,n)]$ represents the covariance between the intensity $I(m,n)$ and the normalized element z, $m \in (1,\ N_G)$, and $n \in (1,\ N_A)$. The relative differences between the first-order approximation and theoretical values are less than 10% if $5D(z) < E(z)$. $D(z)$ and $E(z)$ are the variance and the mean value of M_{11} for every pixel, respectively. We assume that additive Gaussian noise has a zero-mean with the variance σ^2. It is noted that equal angle sets minimize and equalize the estimation variances [9,10,14], and the angles evenly distributed over the half-circle are [9]

$$\theta_i = \frac{(i-1) \times 180^\circ}{N}, \tag{11}$$

where i varies from 1 to N, and the initial positions of the PSG and PSA are 0°. If the polarizer is ideal, we can use the fact that $E(z) = I_0$, $D(z) = 16\sigma^2/(N_G N_A)$; thus, the expression of the variance is

$$D_{\mathrm{Gau}}[R(m,n)] = \frac{\sigma^2}{I_0^2}\left\{1 + \frac{8[2I^2(m,n) - I(m,n)]}{N_G N_A}\right\}, \tag{12}$$

and the covariance is

$$Cov_{\mathrm{Gau}}[R(m,n), R(m',n')] = \frac{4\sigma^2}{I_0^2} \cdot \frac{4I(m,n)I(m',n') - I(m',n') - I(m,n)}{N_G N_A}, \tag{13}$$

where $m \in (1,\ N_G)$, and $n \in (1,\ N_A)$; $m = m'$ and $n = n'$ are not satisfied simultaneously. If we assume that the response matrix has the form diag(1,1,1), the covariance matrix $\mathbf{\Gamma}_{\mathbf{V}_M}$,

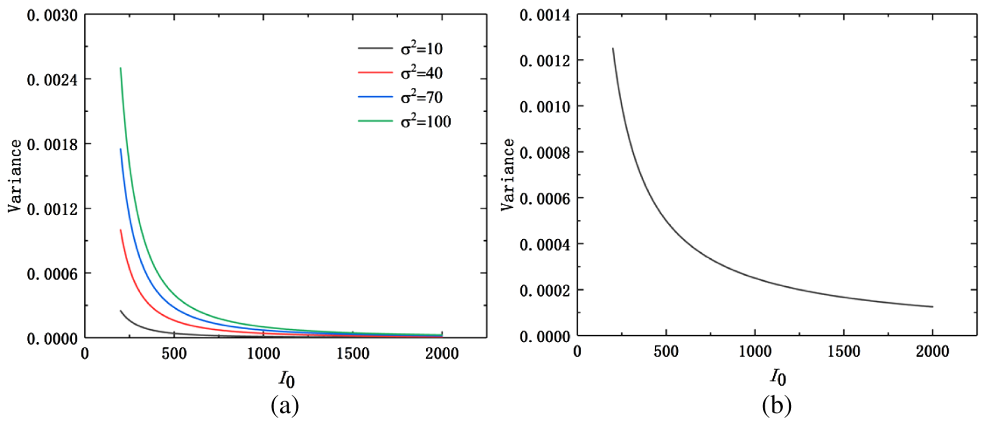

Fig. 1. Theoretical variance coefficient of (a) Gaussian and (b) Poisson noise for different intensities I_0. The configuration of N_G, $N_A = 4$ is considered. The colors are used for different variances of Gaussian noise: $\sigma^2 = 10$ (black), $\sigma^2 = 40$ (red), $\sigma^2 = 70$ (blue), and $\sigma^2 = 100$ (green).

which represents the estimation variances of the response matrix, is

$$VAR[M]_n^{\text{gau}} = \frac{16\sigma^2}{N_G N_A I_0^2}\begin{pmatrix} - & 2 & 2 \\ 2 & 5 & 4 \\ 2 & 4 & 5 \end{pmatrix}, \tag{14}$$

and

$$C_n^{\text{gau}} = \frac{16}{I_0^2}\cdot\frac{26\sigma^2}{N_G N_A}, \tag{15}$$

where $N_G \geqslant 3$, $N_A \geqslant 3$, and the subscript n denotes the results of the normalized response matrix. It is easily seen that the estimation variances of the normalized response matrix increase linearly with $1/I_0^2$, which is much different from the unnormalized matrix (independent with I_0) [14]. Within the maximum DN value of the detector, the estimation variance decreased with an increasing DN value.

The influences of Gaussian noise on the variance coefficient are shown in Fig. 1(a). It is worth noting that Gaussian noise has a great influence on the low source intensity ($I_0 < 500$), and the variance matrix coefficient decreases rapidly with an increasing intensity. This is why Gaussian noise is dominant at low intensities.

We use the property of Poisson noise in which its variance is equal to the mean value, and it is easily seen that $E(z) = I_0$ and $D(z) = 4I_0/(N_G N_A)$. The variance and covariance can be rewritten from Eq. (10):

$$D_{\text{Poi}}[R(m,n)] = \frac{1}{I_0}\left(I - \frac{4I^2(m,n)}{N_G N_A}\right), \tag{16}$$

and

$$Cov_{\text{Poi}}[R(m,n), R(m',n')] = \frac{1}{I_0}\cdot\frac{-4I(m,n)I(m',n')}{N_A N_B}. \tag{17}$$

We use the same assumption to obtain the estimation variances of Poisson noise, and the estimation variance of the response matrix for N_G, $N_A = 3$ is

$$VAR[M]_n^{\text{poi}} = \frac{4}{N_G N_A I_0}\begin{pmatrix} - & 2 & 2 \\ 2 & 4 & 3 \\ 2 & 3 & 4 \end{pmatrix}, \tag{18}$$

for other configurations:

$$VAR[M]_n^{\text{poi}} = \frac{4}{N_G N_A I_0}\begin{pmatrix} - & 2 & 2 \\ 2 & 3 & 4 \\ 2 & 4 & 3 \end{pmatrix}, \tag{19}$$

and

$$C_n^{\text{poi}} = \frac{4}{I_0}\cdot\frac{22}{N_G N_A}. \tag{20}$$

It can be noted that the variance matrix of Poisson noise is inversely proportional to the intensity I_0 (linear with I_0 for an unnormalized matrix [14]); therefore, the DN values have less influence on the estimation variance compared with Gaussian noise. In other words, if the DN value is low enough, the dominant noise is considered to be a Gaussian distribution. In contrast, if the DN value is strong enough, the dominant noise is a Poisson distribution ($I_0 \gg 4\sigma^2$), as shown in Fig. 1(b).

These two types of noise jointly influence the precision under practical conditions; therefore, Gaussian and Poisson noise are used to study the variations in estimation the variance. The property of variance is described as

$$VAR[M]_n^s = VAR[M]_n^{\text{gau}} + VAR[M]_n^{\text{poi}}, \tag{21}$$

where the superscript S denotes the sum of the estimation variance in the presence of Gaussian and Poisson noise. For the configuration of 3×3, $VAR[M]^s(2,2)$ and $VAR[M]^s(3,3)$ have the same value $(6I_0 + 20\sigma^2)/(N_G N_A I_0^2)$. For other configurations, $VAR[M]^s(2,2)$ and $VAR[M]^s(3,3)$ are $(8I_0 + 20\sigma^2)/(N_G N_A I_0^2)$; in contrast, $VAR[M]^s(2,3)$ and $VAR[M]^s(3,2)$ are $(6I_0 + 16\sigma^2)/(N_G N_A I_0^2)$. After substituting Eqs. (14), (18), and (19) into Eq. (21), it can easily be seen that the total estimation variance matrix can be written as $N_G = 3$, $N_A = 3$:

$$VAR[M]_n^s = \frac{4I_0 + 16\sigma^2}{N_G N_A I_0^2}\begin{pmatrix} - & 2 & 2 \\ 2 & \frac{4I_0+20\sigma^2}{I_0+4\sigma^2} & \frac{3I_0+16\sigma^2}{I_0+4\sigma^2} \\ 2 & \frac{3I_0+16\sigma^2}{I_0+4\sigma^2} & \frac{4I_0+20\sigma^2}{I_0+4\sigma^2} \end{pmatrix}, \tag{22}$$

and for other configurations:

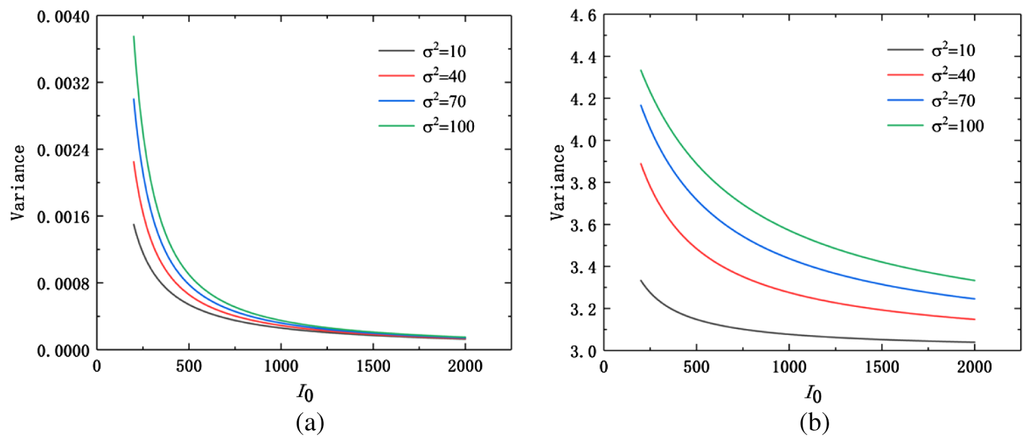

Fig. 2. Theoretical variance (a) coefficient and (b) M_{22}/M_{33} for different intensities I_0. The colors are used for different variances of Gaussian noise: $\sigma^2 = 10$ (black), $\sigma^2 = 40$ (red), $\sigma^2 = 70$ (blue), and $\sigma^2 = 100$ (green).

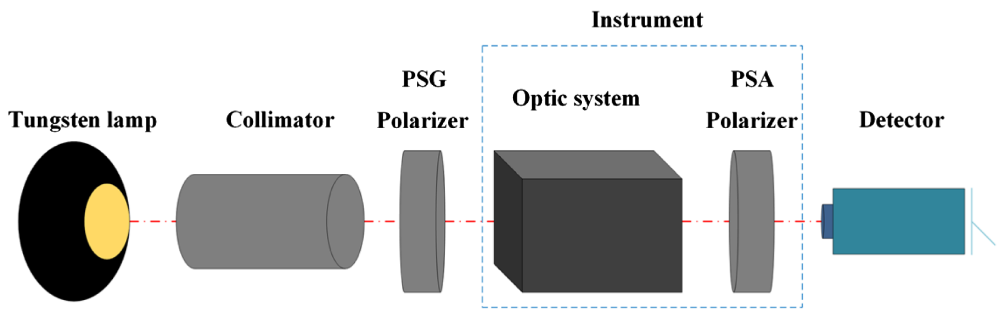

Fig. 3. Optical schema for the verification of the calibration strategy.

$$VAR[M]^s_n = \frac{4I_0 + 16\sigma^2}{N_G N_A I_0^2}\begin{pmatrix} - & 2 & 2 \\ 2 & \frac{3I_0+20\sigma^2}{I_0+4\sigma^2} & 4 \\ 2 & 4 & \frac{3I_0+20\sigma^2}{I_0+4\sigma^2} \end{pmatrix}. \quad \textbf{(23)}$$

With the increase of the variance of Gaussian noise, the elements $VAR[M]^s(2, 2)$, $VAR[M]^s(3, 3)$, $VAR[M]^s(3, 2)$, and $VAR[M]^s(2, 3)$ of the configuration of 3×3 and the elements $VAR[M]^s(2, 2)$, $VAR[M]^s(3, 3)$ of the others increase, which is the key to verifying the theory from the experiments. The theoretical results disturbed by two types of noise are illuminated in Fig. 2. If the maximum DN value is beyond 1000, the influence of Gaussian noise is considered to be negligible with $\sigma^2 = 100(< 16.7\%)$, and the dominant noise is a Poisson distribution. We can measure the noise of the detector in advance and choose the suitable configuration and intensity value that provide the required precision.

Next, we will illuminate the conclusion of the experiments.

4. EXPERIMENTS

A. Experimental Setups

The PSG and PSA have the same component and are composed of a polarizer (CODIXX, COLORPOL-VIS-600-BC5). One of them can be rotated 360° via a motorized rotation stage (Zolix, RAK100), and the other can be rotated by a manual rotation stage (Zolix, KSMR5A-120). The light beam emitted from the tungsten lamp as a point source passes through two polarizers. A spike filter will be used at 700 nm with the collimator parallel to the incident light. The extinction ratio of the polarizer is less than 1:100000 in 700 nm. The intensity fluctuations were checked to be negligible (approximately <0.5% in half an hour). A complementary metal oxide semiconductor (CMOS) camera (Ximea, MQ042CG-CM) with 100×100 pixels is employed to calculate the normalized variance.

We employ the configuration of $N_G = 4$, $N_A = 4$ ($\theta_{N_A(N_G)} = 0°, 45°, 90°, 135°$), with the experimental setup shown in Fig. 3. According to the full well capacity and 10 bit analog-to-digital converter, the relationship between the DN value and the number of electrons is $13e^{-1}$/DN. First, we let the maximum DN value passing through the PSA be approximately 900 by regulating the voltage of the tungsten lamp, and the exposure time is kept at 28 ms. For the 10 bit analog-to-digital converter, this DN value (900) is large enough. During the experiments, we decrease the DN value by approximately 100 each time until the minimum DN value is 200. A Newtonian telescopic system is then employed to create the real calibration environment and to verify whether the conclusion can be applicable under the condition of an off-diagonal response matrix.

B. Results and Discussion

To evaluate the performance of the polarization calibration, no component between the PSG and the PSA is used to ensure the validity of the experiment. M_{os} represents the response matrix of

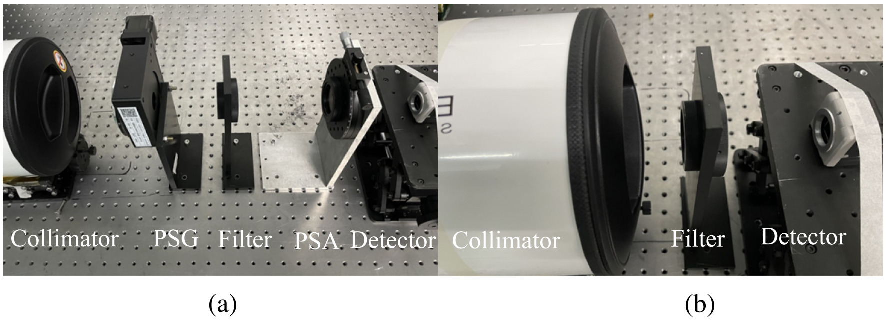

Fig. 4. Photograph of the experimental setup for (a) no component but air between the PSG and PSA and (b) the measurement of CMOS noise. The devices are (a) collimator, PSG, spike filter, PSA, and CMOS and (b) collimator, spike filter, and CMOS from left to right.

the optical system, and M_{no} represents that of no component but air between the PSG and PSA shown in Fig. 4(a). More than 100 measurements are performed, and the response matrix is

$$M_{no}=\begin{pmatrix}1 & 0 & 0.002\\ 0.004 & 0.996 & -0.005\\ -0.003 & -0.002 & 0.997\end{pmatrix}. \quad (24)$$

Equation (24) is close to the ideal diagonal matrix, which demonstrates the validity of the experiment. The response matrix of a Newtonian telescopic system is

$$M_{os}=\begin{pmatrix}1 & -0.052 & 0.026\\ -0.013 & 0.98 & 0.091\\ 0.027 & -0.053 & 0.95\end{pmatrix}. \quad (25)$$

The combination of a tungsten lamp, a collimator, filter, and CMOS camera is used to determine the σ_{DN}^2 in dark field shown in Fig. 4(b), and the mean/variance of DN is equal to 17.5/5.8 with 20 repeated measurements. The variance of the DN value corresponding to Poisson noise can be approximately considered to be one-tenth of the DN value shown in Fig. 5. One notices that the detector parameters for the measurement of Poisson noise are consistent with those for polarization calibration, which can reduce the step of conversion between the number of electrons and DN value. Therefore, the variance can be conveniently described by the DN value in this experiment.

According to the experimental results, the variance matrix can be rewritten from Eq. (23):

$$VAR[M]_n^s=\frac{2I_0+80\sigma^2}{5N_GN_AI_0^2}\begin{pmatrix}- & 2 & 2\\ 2 & \frac{3I_0+200\sigma^2}{I_0+40\sigma^2} & 4\\ 2 & 4 & \frac{3I_0+200\sigma^2}{I_0+40\sigma^2}\end{pmatrix}. \quad (26)$$

The variances of the response matrix consist of the matrix coefficient $(2I_0+80\sigma^2)/(5N_GN_AI_0^2)$ and the matrix elements. The elements $VAR[M]^s(2,2)$ and $VAR[M]^s(3,3)$ are less than those of Eq. (23), since the noise is lower compared with theory. We substitute the intensities I_0 of the eight groups, ranging from 200 to 900 into Eq. (26). The theoretical and experimental results of the matrix coefficient are shown in Fig. 6. The matrices for the estimation variance are described in Table 1. The relative differences between the theoretical and experimental results are less than 11.7% for the coefficient of the variance matrix and 5.3% for the element. With the increase of intensity I_0, the variances decrease gradually. The variances of the matrix element are shown in Fig. 7. It can be seen that the variance of M_{11} is 0 due to the normalization. The variances of M_{22} and M_{33} decrease with I_0; in contrast, the variances of the other elements are nearly constant (2 or 4) shown in Fig. 7.

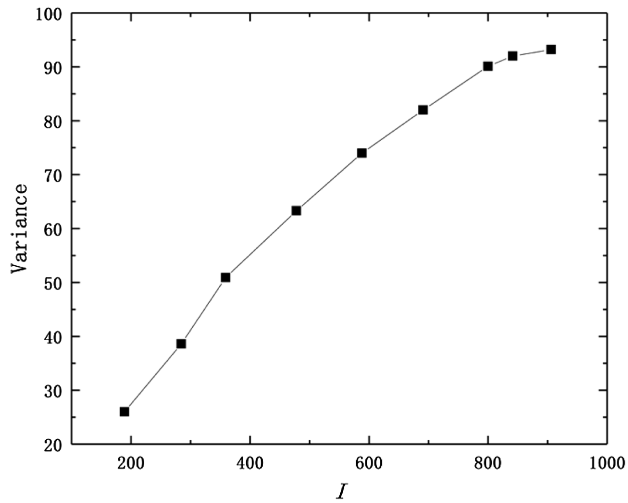

Fig. 5. Changes of the variance with the number of the DN value of the CMOS camera.

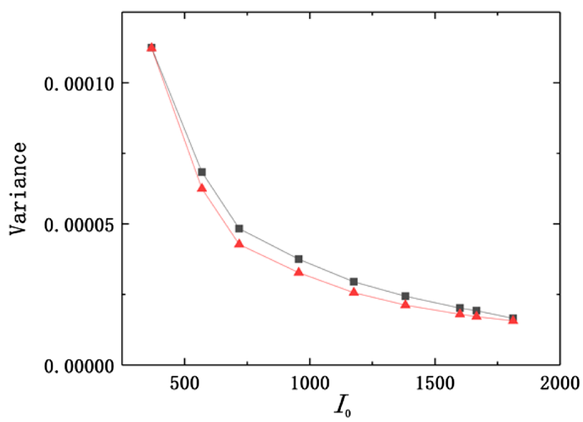

Fig. 6. Changes in the response matrix coefficient with the source intensity I_0. The red lines show the predictable results, whereas the black lines show the measurement results.

Table 1. Theoretical and Experimental Variance Matrix for Different I_0[a]

	Experimental Matrix	Theoretical Matrix	Experimental Matrix	Theoretical Matrix	Experimental Matrix	Theoretical Matrix
$VAR[M] = V_{1-3} \times V_{1-3}$	$\begin{pmatrix} 0 & 2.03 & 1.98 \\ 2.03 & 3.89 & 3.93 \\ 1.96 & 3.82 & 3.58 \end{pmatrix}$ 1.15×10^{-4}	$\begin{pmatrix} 0 & 2.00 & 2.00 \\ 2.00 & 3.78 & 4.00 \\ 2.00 & 4.00 & 3.78 \end{pmatrix}$ 1.12×10^{-4}	$\begin{pmatrix} 0 & 2.02 & 1.99 \\ 2.03 & 3.85 & 3.87 \\ 1.97 & 3.89 & 3.71 \end{pmatrix}$ 6.83×10^{-5}	$\begin{pmatrix} 0 & 2.00 & 2.00 \\ 2.00 & 3.59 & 4.00 \\ 2.00 & 4.00 & 3.59 \end{pmatrix}$ 6.25×10^{-5}	$\begin{pmatrix} 0 & 2.02 & 1.99 \\ 2.02 & 3.52 & 3.97 \\ 1.97 & 3.84 & 3.47 \end{pmatrix}$ 4.83×10^{-5}	$\begin{pmatrix} 0 & 2.00 & 2.00 \\ 2.00 & 3.48 & 4.00 \\ 2.00 & 4.00 & 3.48 \end{pmatrix}$ 4.27×10^{-5}
$VAR[M] = V_{4-6} \times V_{4-6}$	$\begin{pmatrix} 0 & 2.02 & 1.99 \\ 2.04 & 3.58 & 4.03 \\ 1.96 & 3.82 & 3.39 \end{pmatrix}$ 3.75×10^{-5}	$\begin{pmatrix} 0 & 2.00 & 2.00 \\ 2.00 & 3.40 & 4.00 \\ 2.00 & 4.00 & 3.40 \end{pmatrix}$ 3.27×10^{-5}	$\begin{pmatrix} 0 & 2.01 & 1.99 \\ 2.03 & 3.45 & 4.09 \\ 1.97 & 3.91 & 3.34 \end{pmatrix}$ 2.95×10^{-5}	$\begin{pmatrix} 0 & 2.00 & 2.00 \\ 2.00 & 3.34 & 4.00 \\ 2.00 & 4.00 & 3.34 \end{pmatrix}$ 2.56×10^{-5}	$\begin{pmatrix} 0 & 2.01 & 2.00 \\ 2.02 & 3.35 & 4.16 \\ 1.97 & 3.99 & 3.30 \end{pmatrix}$ 2.44×10^{-5}	$\begin{pmatrix} 0 & 2.00 & 2.00 \\ 2.00 & 3.30 & 4.00 \\ 2.00 & 4.00 & 3.30 \end{pmatrix}$ 2.12×10^{-5}
$VAR[M] = V_{7-9} \times V_{7-9}$	$\begin{pmatrix} 0 & 2.01 & 2.00 \\ 2.01 & 3.24 & 4.03 \\ 1.98 & 4.12 & 3.23 \end{pmatrix}$ 2.01×10^{-5}	$\begin{pmatrix} 0 & 2.00 & 2.00 \\ 2.00 & 3.26 & 4.00 \\ 2.00 & 4.00 & 3.26 \end{pmatrix}$ 1.80×10^{-5}	$\begin{pmatrix} 0 & 1.99 & 2.02 \\ 2.01 & 3.16 & 4.15 \\ 1.99 & 4.16 & 3.22 \end{pmatrix}$ 1.92×10^{-5}	$\begin{pmatrix} 0 & 2.00 & 2.00 \\ 2.00 & 3.25 & 4.00 \\ 2.00 & 4.00 & 3.25 \end{pmatrix}$ 1.72×10^{-5}	$\begin{pmatrix} 0 & 1.98 & 2.03 \\ 2.00 & 3.05 & 4.06 \\ 2.00 & 4.09 & 3.11 \end{pmatrix}$ 1.65×10^{-5}	$\begin{pmatrix} 0 & 2.00 & 2.00 \\ 2.00 & 3.23 & 4.00 \\ 2.00 & 4.00 & 3.23 \end{pmatrix}$ 1.56×10^{-5}

[a]Each $V_1 - V_9$ corresponds to a I_0 (368, 569, 718, 956, 1176, 1382, 1600, 1666, 1812).

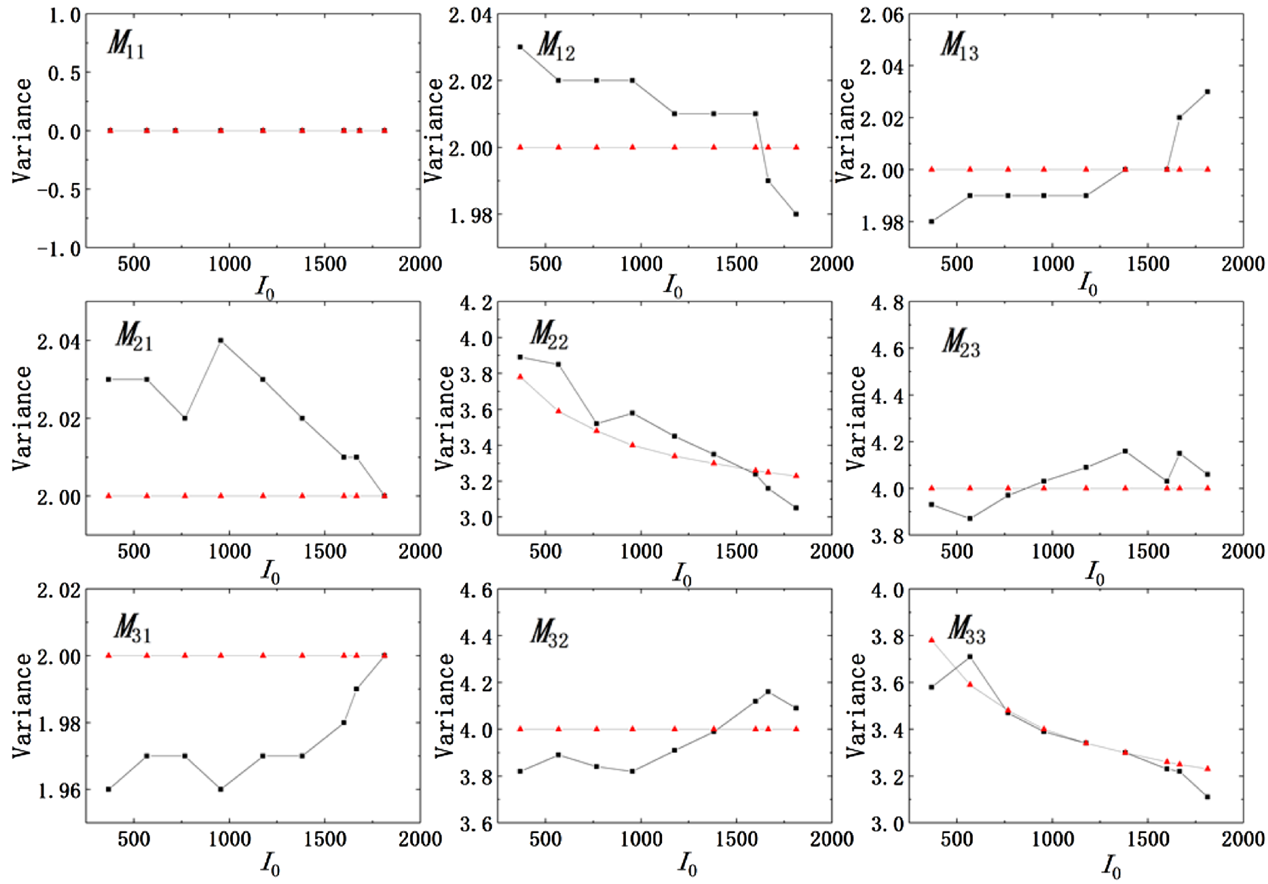

Fig. 7. Changes in the variance of the response matrix element with source intensity I_0. The red lines show the predicted results, whereas the black lines show the measurement results.

The experimental results are in good agreement with the theoretical prediction values for the matrix coefficient and element. Therefore, the theoretical model can predict the calibration precision well. If 10^{-4} (1% standard deviation) is required for the variance, the configuration of $N_G = 4$, $N_A = 4$, and $I_0 = 1200$ can be chosen according to Eq. (26). When the numbers of illumination (N_G) and analysis (N_A) states are greater than 4, the value of I_0 will be decreased; for example, the configuration of $N_G = 5$, $N_A = 5$, and $I_0 = 820$ should be employed.

Additionally, the dominant noise is Poisson noise because M_{22} and M_{33} are close to 3 in terms of the strong source intensity ($I_0 > 1500$) shown in Fig. 7. The product of the coefficient and element is the variance of $M_{12} - M_{33}$. With the increase of I_0, the coefficient and element of M_{22}/M_{33} are decreased, and variance of $M_{22} - M_{33}$ is decreased. It must be noticed that Poisson noise is still dominant for $I_0 \approx 400$ due to the small variance σ^2 of Gaussian noise. We can choose the suitable source

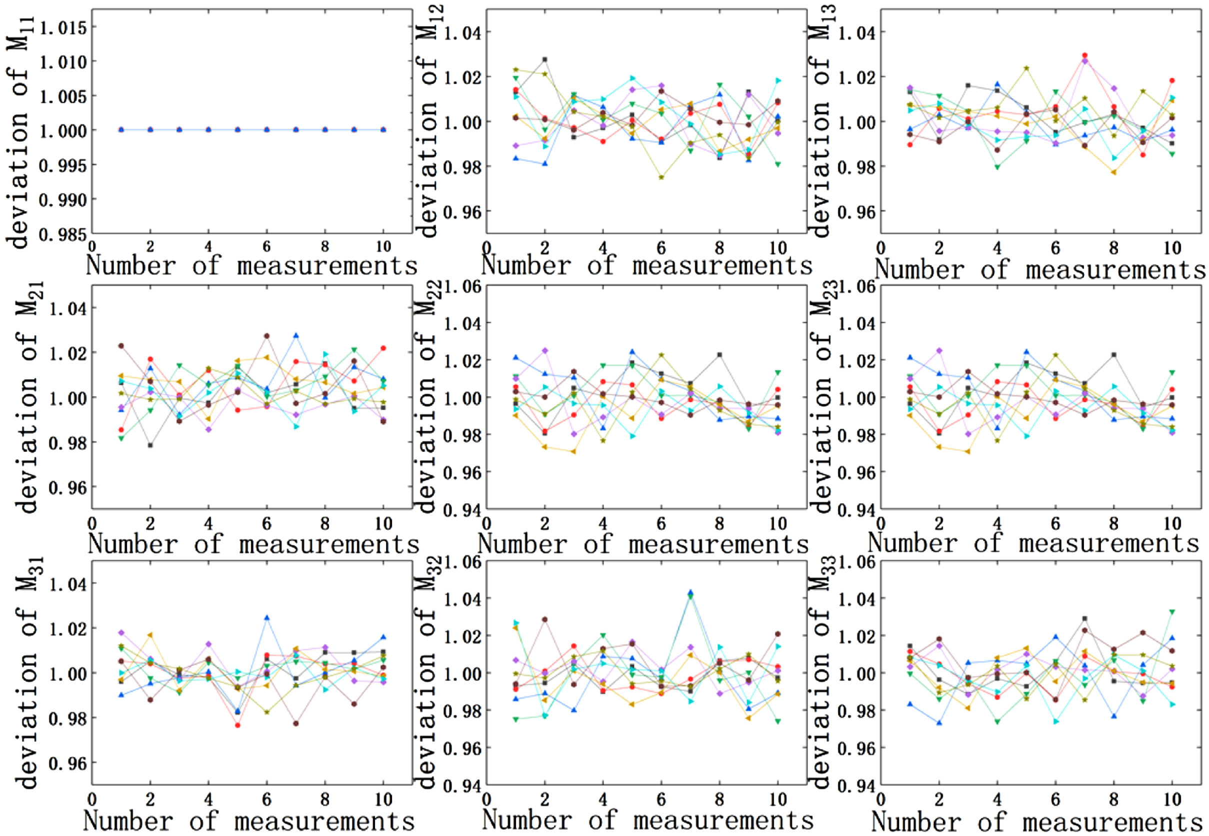

Fig. 8. Deviation of 10 repeated measurements for the different I_0 368 (gray), 569 (red), 718 (dark blue), 956 (green), 1176 (brown), 1382 (purple), 1600 (yellow), 1666 (blue), and 1812 (dark green) on the response matrix ($M_{11} - M_{33}$). Each estimation variance is normalized by the mean value of variance for 10 measurements.

intensity I_0 and calibration configurations according to the requirements when the noise of the detector is measured.

C. Systematic Error

During the derivation of the theory, we only consider the influence of Gaussian and Poisson noise. However, the calibration precision will deviate from the theoretical prediction in practice due to other types of noise (such as uniform noise, salt & pepper noise, and compound noise) and errors. Figure 6 shows that the variance matrix coefficient of the experiment is larger than the one of theory. Moreover, the difference is less than 16% for the sum of the variance matrix. This means that Gaussian and Poisson noise are dominant in these measurements. It can be ensured that the rotation error of the polarizer is less than 0.1°, and the angle error between the PSG and PSA is 0.1°. Although all parts are completely fixed, there can be a slight change in the orientation of the PSG and PSA, which influence the variance. Combined with the relative deviation of 1% in Eq. (24) and 16% for the sum of the variance matrix, the systematic errors have no significant influence on the experiment.

Ten repeated measurements were made to obtain the measurement precision for the errors, as shown in Fig. 8. The relative differences in 10 repeated measurements are found to be less than 2.8% for the variation of M_{12}, M_{13}, M_{21}, and M_{31} and 4.1% for the variation of M_{22}, M_{23}, M_{32}, and M_{33}, respectively. The variances fluctuate due to the randomness of noise (Gaussian, Poisson, other types of noise, errors), which causes the 4.1% variation in the 10 repeated measurements. This means that small systematic errors and other noise have no significant influence and are less than the influence of change of I_0 (about 17% for M_{22} and M_{33}) in the polarization calibration, which can ensure the validity of the experiment.

5. CONCLUSION

We have studied the estimation variance of the normalized response matrix and analyzed the influences of the source intensity, noise, and calibration configuration. Moreover, the theoretical prediction model of polarization calibration is built. The experiments show that the relative changes between the theoretical prediction and experimental results are less than 16%, and the model can be adopted to choose the optimal configurations that provide the required precision.

The method is useful for arbitrary linear polarization calibration, and we assess their fundamental limits in the presence of Gaussian and Poisson noise. We will focus on the influence of every element on the estimation variance in the future.

Funding. Joint Fund of Astronomy (U1931118); Chinese Academy of Sciences Strategic Pioneer Program on Space Science (XDA15320000, XDA15320100, XDA15320103); Joint Research Fund in Astronomy under cooperative agreement between the National Natural Science Foundation of China (NSFC) and the Chinese Academy of Sciences (CAS) (U2031122).

Acknowledgment. The authors thank the X-ray and EUV optics technology laboratory in the Changchun Institute of Optics, Fine Mechanics and Physics (CIOMP) for supporting this research.

Disclosures. The authors declare no conflicts of interest.

Data availability. Data underlying the results presented in this paper are not publicly available at this time but may be obtained from the authors upon reasonable request.

REFERENCES

1. T. G. Moran, J. M. Davila, J. S. Morrill, D. Wang, and R. Howard, "Solar and heliospheric observatory/large angle spectrometric coronagraph polarimetric calibration," Sol. Phys. **237**, 211–222 (2006).
2. R. Howard, J. Moses, A. Vourlidas, J. Newmark, D. Socker, S. Plunkett, C. Korendyke, J. Cook, A. Hurley, and J. Davila, "Sun Earth connection coronal and heliospheric investigation (SECCHI)," Space Sci. Rev. **136**, 67 (2008).
3. G. Giono, R. Ishikawa, N. Narukage, R. Kano, Y. Katsukawa, M. Kubo, S. Ishikawa, T. Bando, H. Hara, and Y. Suematsu, "Polarization calibration of the Chromospheric Lyman-Alpha SpectroPolarimeter for a 0.1% polarization sensitivity in the VUV range. Part I: Pre-flight calibration," Sol. Phys. **291**, 3831–3867 (2016).
4. Y. Fu, Z. Huang, H. He, H. Ma, and J. Wu, "Flexible 3×3 Mueller matrix endoscope prototype for cancer detection," IEEE Trans. Instrum. Meas. **67**, 1700–1712 (2018).
5. M. Garcia and V. Gruev, "Optical characterization of rigid endoscopes and polarization calibration methods," Opt. Express **25**, 15713–15728 (2017).
6. H. Mcnairn and B. Brisco, "The application of C-band polarimetric SAR for agriculture: a review," Can. J. Remote Sens. **30**, 525–542 (2014).
7. J. S. Tyo, D. L. Goldstein, D. B. Chenault, and J. A. Shaw, "Review of passive imaging polarimetry for remote sensing applications," Appl. Opt. **45**, 5453–5469 (2006).
8. G. Giono, R. Ishikawa, N. Narukage, R. Kano, Y. Katsukawa, M. Kubo, S.-N. Ishikawa, T. Bando, H. Hara, and Y. Suematsu, "Polarization calibration of the chromospheric lyman-alpha spectropolarimeter for a 0.1% polarization sensitivity in the VUV range. Part II: In-flight calibration," Sol. Phys. **292**, 57 (2017).
9. M. R. Foreman, A. Favaro, and A. Aiello, "Optimal frames for polarization state reconstruction," Phys. Rev. Lett. **115**, 263901 (2015).
10. F. Goudail and A. Bénière, "Estimation precision of the degree of linear polarization and of the angle of polarization in the presence of different sources of noise," Appl. Opt. **49**, 683–693 (2010).
11. G. Anna and F. Goudail, "Optimal Mueller matrix estimation in the presence of Poisson shot noise," Opt. Express **20**, 21331–21340 (2012).
12. F. Goudail, "Optimal Mueller matrix estimation in the presence of additive and Poisson noise for any number of illumination and analysis states," Opt. Lett. **42**, 2153–2156 (2017).
13. T. Mu, D. Bao, C. Zhang, Z. Chen, and J. Song, "Optimal reference polarization states for the calibration of general Stokes polarimeters in the presence of noise," Opt. Commun. **418**, 120–128 (2018).
14. X. Li, B. Chen, L. He, and X. Gao, "Optimal configurations for different incident polarization states in linear polarization calibration," Appl. Opt. **59**, 9520–9531 (2020).
15. A. N. Langville and W. J. Stewart, "The Kronecker product and stochastic automata networks," J. Comput. Appl. Math. **167**, 429–447 (2004).
16. F. Goudail, "Noise minimization and equalization for Stokes polarimeters in the presence of signal-dependent Poisson shot noise," Opt. Lett. **34**, 647–649 (2009).
17. M. Bass and V. N. Mahajan, *Handbook of Optics, Volume I: Geometrical and Physical Optics, Polarized Light, Components and Instruments* (McGraw-Hill, 2010).